A numerical study of the target system of an ADSS with different flow guides

K ARUL PRAKASH[1], B V RATHISH KUMAR[2] and G BISWAS[1]

[1]Department of Mechanical Engineering; [2]Department of Mathematics, Indian Institute of Technology, Kanpur 208 016, India

E-mail: arulk@iitk.ac.in; gtm@iitk.ac.in

Abstract. The mechanical design of the target module of an accelerator driven sub-critical nuclear reactor system (ADSS) calls for an analysis of the related thermal-hydraulic issues because of large amount of heat deposition in the spallation region during the course of nuclear interactions with the molten lead bismuth eutectic (LBE) target. The LBE also should carry the entire heat generated as a consequence of the spallation reaction. The problem of heat removal by the LBE is a challenging thermal-hydraulic issue. For this, one has to examine the flows of low Prandtl number fluids (LBE) in a complex ADSS geometry. In this study, the equations governing the laminar flow and thermal energy are solved numerically using the streamline upwind Petrov–Galerkin (SUPG) finite element (FE) method. The target systems with a straight and a nozzle guide have been considered. The principal purpose of the analysis is to trace the flow and temperature distribution and thereby to check the suitability of the flow guide in avoiding the recirculation or stagnation zones in the flow space that may lead to hot spots.

1. Introduction

In the near future, ADSS will play a significant role as an alternative source of power generation. ADSS possesses high potential for nuclear radioactive waste transmutation and operates in sub-critical conditions [1]. In an ADSS, a high-energy proton beam from an accelerator irradiates a target, which is basically a flowing heavy density liquid metal (LBE). As a result, the liquid metal produces spallation neutrons that initiate a fission reaction in the sub-critical core. ADSS has two sections: (1) the downcomer, incoming (2) the riser, outlet. The protons are induced on the target through a vacuum pipe closed by a window at the end. Therefore, the beam window is subject to high heat fluxes, thermal and mechanical stresses. A large amount of spallation heat is deposited on the window and in the LBE. Though it is relatively easy to remove the total spallation heat by the LBE,
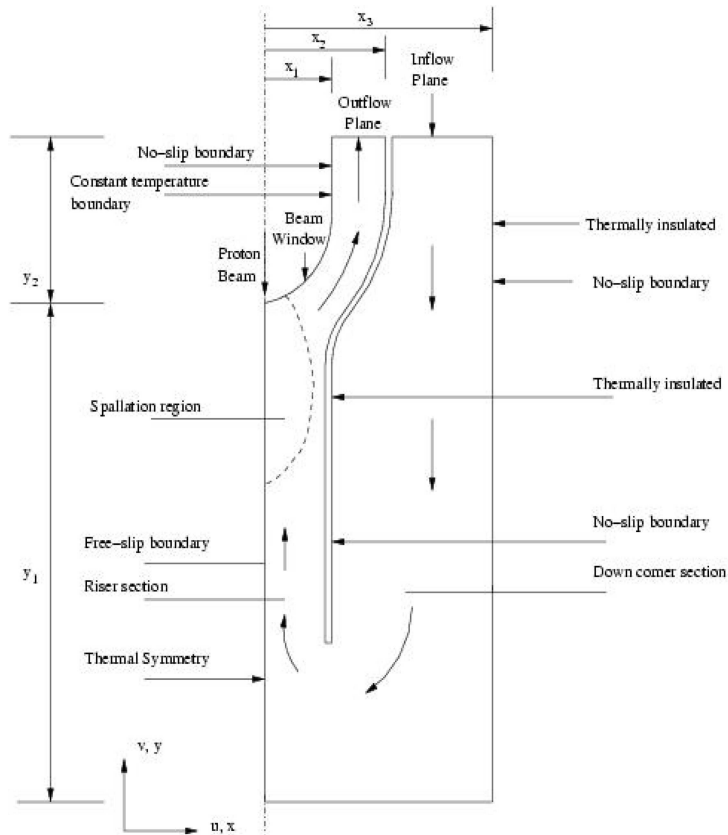
Figure 1. Physical domain of the spallation target system of an ADSS with straight flow guide.

it is crucial to achieve this without the target temperature exceeding the stipulated temperature in any region of the flow. There should not be any recirculation or stagnation zones leading to the hot spots, inadequate window cooling, generation of vapors etc. This necessitates a detailed flow analysis in the spallation region, flow region near the entrance of the annular zone along with the determination of temperature distribution in the ADSS geometry.

The thermal-hydraulic behavior of a liquid metal spallation region may be examined in either of the two ways: The first option is to build a full-size target and install it in a proton beam, suitably supplied with coolant under design conditions and instrumented. The second is to simulate such a target using a state-of-the-art computational fluid dynamics (CFD) tool. The second option is adopted in the study. Different geometric designs of LBE-based ADSS are presently under consideration all over the world. The current status in the development of ADSS is presented by Maiorino *et al* [2]. However, each of these models warrants a thorough investigation. Careful numerical experiments are needed to identify the flow stagnation and recirculation zones in the complex ADSS geometry.
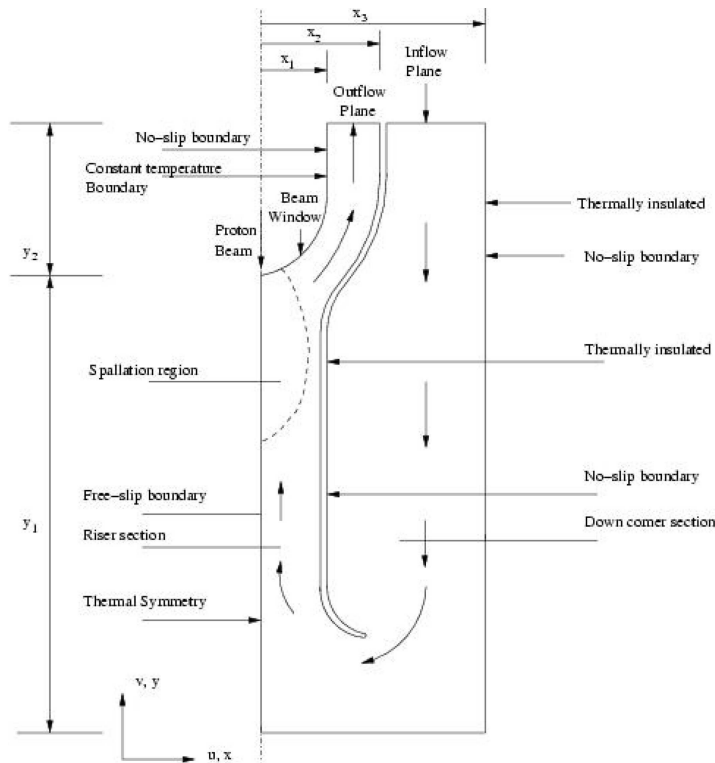
Figure 2. Physical domain of the spallation target system of an ADSS with the nozzle-shaped flow guide.

A review of the recent literature reveals that there have been few investigations focussing on the window region of an ADSS. Dury *et al* [3] have analyzed the spallation zone near the beam window of the European spallation source liquid-metal target facility numerically using CFX-4. They considered liquid mercury as the spallation target. Cho *et al* [4] have computed the heat transfer and flow characteristics in a simplified version of the spallation zone of an axisymmetric ADSS model called HYPER using ANSYS and CFX packages. While there is a circular flow guide in ADSS model considered by Dury *et al* [3], there is no such flow guide in the model studied by Cho *et al* [4]. Recently, window-based ADSS models, such as, XADS [5] with nozzle-shaped flow guides have been proposed. In this model, the downcomer part of the ADSS is separated from the riser part by using a flow guide. The flow takes a 180° turn around the tip of the flow guide.

Therefore, in this paper we consider the entire target system of an ADSS model with a straight flow guide (figure 1) or a nozzle-shaped flow guide (see figure 2). In view of the continuous high energetic proton beam impingement on the target, window surface may be assumed to be isothermal boundary. An in-house SUPG-FEM code based on the projection scheme of Chorin [6] has been developed and validated. Simulations have been carried out to analyze the flow and heat transfer characteristics in the ADSS geometry for a wide range of Reynolds numbers.

2. Governing equations and solution scheme

2.1 *Governing equations*

The flow is considered to be viscous, incompressible and laminar. The geometry of interest is axisymmetric in nature. The physical domain of the target system of ADSS with boundary conditions are shown in figures 1 and 2. Uniform velocity profile is given as inlet. The computational domain is discretized into small quadrilateral elements. The velocity components, pressure, temperature are collocated at each node of the element. The dimensionless equations governing the two-dimensional plane or axisymmetric mean flow of an incompressible fluid [7,8] are

Continuity equation

$$\frac{1}{x^j}\frac{\partial}{\partial x}(x^j u) + \frac{\partial v}{\partial y} = 0. \tag{1}$$

Momentum equation

$$\frac{\partial u}{\partial \tau} + \left[u\frac{\partial u}{\partial x} + v\frac{\partial u}{\partial y} \right] = -\frac{\partial p}{\partial x} + \frac{1}{x^j}\frac{1}{\mathrm{Re}}$$
$$\times \left[\frac{\partial}{\partial x}\left(x^j\frac{\partial u}{\partial x} \right) + \frac{\partial}{\partial y}\left(x^j\frac{\partial u}{\partial y} \right) \right], \tag{2}$$

$$\frac{\partial v}{\partial \tau} + \left[u\frac{\partial v}{\partial x} + v\frac{\partial v}{\partial y} \right] = -\frac{\partial p}{\partial y} + \frac{1}{x^j}\frac{1}{\mathrm{Re}}$$
$$\times \left[\frac{\partial}{\partial x}\left(x^j\frac{\partial v}{\partial x} \right) + \frac{\partial}{\partial y}\left(x^j\frac{\partial v}{\partial y} \right) \right], \tag{3}$$

where p is the non-dimensional pressure and (u, v) are the non-dimensional velocity components in the coordinates (x, y) which for the axisymmetric flows are the radial and axial coordinates respectively. Therefore, these equations describe plane flows on setting $j = 0$ and axisymmetric flows on setting $j = 1$.

Energy equation

$$\frac{\partial \theta}{\partial \tau} + u\frac{\partial \theta}{\partial x} + v\frac{\partial \theta}{\partial x} = \frac{1}{x^j}\frac{1}{\mathrm{Re}\,\mathrm{Pr}}\left[\frac{\partial}{\partial x}\left\{ x^j\frac{\partial \theta}{\partial x} \right\} + \frac{\partial}{\partial y}\left\{ x^j\frac{\partial \theta}{\partial y} \right\} \right],$$
$$\mathrm{Re} = \frac{V_0 D}{\nu}, \quad \mathrm{Pr} = \frac{\nu}{\alpha}, \tag{4}$$

where D is the characteristic length, ν is kinematic viscosity, α is thermal diffusivity and V_0, the mean inlet velocity.

2.2 *Eulerian velocity correction approach*

This method is essentially based on the projection scheme of Chorin [6], which was originally developed in a finite difference context and identical to Marker and Cell (MAC) method of Harlow and Welch [9]. This has been extended to 2D finite element method by Donea *et al* [10].

In the present study, the algorithm has been extended to the axisymmetric solution. The solution for each time step is obtained through the following four steps.

1. Calculation of provisional velocities.
2. Solution of pressure equation.
3. Velocity correction.
4. Calculation of temperature distribution.

An incomplete Cholesky preconditioned conjugate residual method is used to solve the pressure Poisson equation. A steady solution is obtained through pseudo-time marching. Finally, the energy equation (4) is solved with the steady state velocity field to obtain the temperature distribution.

3. Formulation

The detailed weak formulation and finite element formulation has been presented in Maji and Biswas [11]. The trial functions are piecewise bilinear. The four noded quadrilateral elements are mapped on a $(2 \star 2)$ square using isoparametric transformation. SUPG technique of Brooks and Hughes [12] is used based on the notion that upwind biasing is effectively equivalent to introduction of an artificial diffusion in the flow direction.

4. Grid generation and code validation

The computational grid is generated using algebraic method and smoothened and clustered by elliptic partial grid generation technique using Poisson's equations. The outer domain and the computational grid for the straight flow guide and nozzle-shaped guide are shown in figures 3 and 4. In order to validate our in-house SUPG-FE code, it is tested on three benchmark problems, namely the flow in a lid-driven cavity, the flow over a backward-facing step and the buoyancy-driven cavity flow. Our grid-independent results for these problems are compared with the results available in the literature and found to be in good agreement.

5. Results and discussions

Figure 5 shows streamline patterns for the target system having straight flow guide for Re = 500, 700 and 1000. At Re = 500, a primary vortex is observed near the inlet section along the guide due to sudden expansion of the flow domain. In
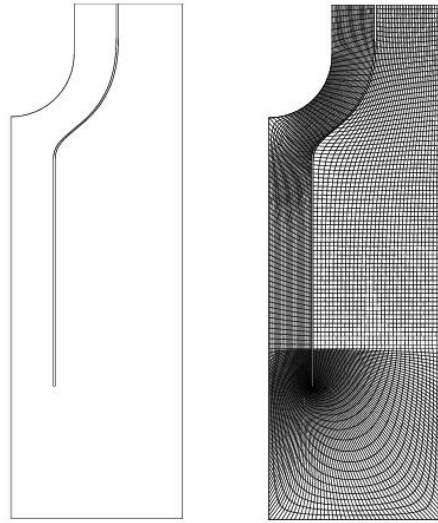
Figure 3. Outer domain and computational grid of the target system with the straight flow guide.
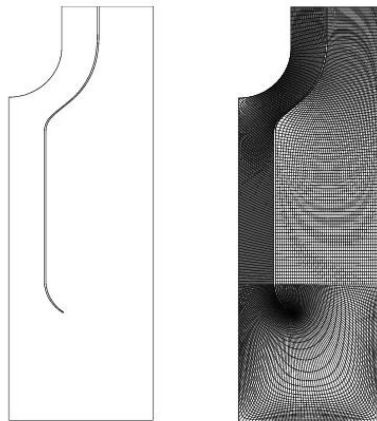

Figure 4. Outer domain and computational grid of the target system with the nozzle-shaped flow guide.

addition, recirculation regions are observed in the riser section starting from 180°, turn all along the flow guide and also near to the exit plane along both the beam window and the flow guide. At Re = 700 and 1000, the size of the primary vortex decreases due to increasing velocity field and multiple vortices are created in the recirculation region in the riser section along the flow guide. The flow separation and formation of the vortices near the inlet section and close to the exit plane can be attributed to the expansion of the flow passage establishing an adverse pressure gradient therein. Near the tip of the flow guide, the fluid experiences a sudden change (180°) in direction. The higher velocity fluid moves towards the outer wall
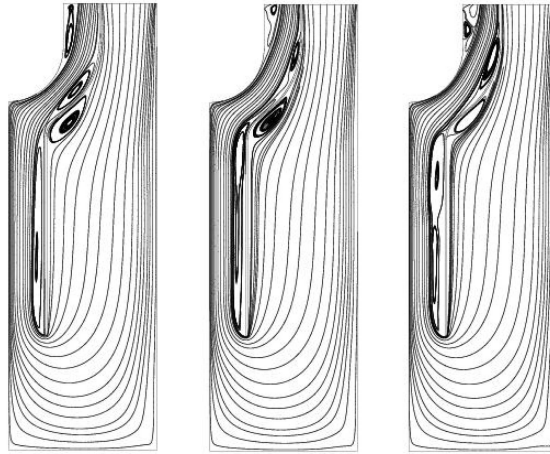
Figure 5. Streamline plots of the target system of an ADSS with straight flow guide for Re = 500, 700 and 1000.

under the influence of centrifugal force. The momentum of the fluid near the inner side (here it is the flow guide) decreases. The low momentum of the fluid on the flow guide eventually leads to a flow separation and reversal.

For all the Reynolds numbers, pressure (figure 6) is seen to increase near the zone of sudden expansion immediately after the inlet. Subsequently, it decreases uniformly in the straight part of the flow passage up to the bend. The pressure drop and thereby the pressure gradient is very high close to the 180° turn. Thereafter, the pressure recovers up to the concave downstream, where secondary recirculation zone occurs and finally the fluid attains the atmospheric pressure at the exit plane.

The temperature contours for the isothermal window boundary for different Reynolds numbers are shown in figure 7. In almost all the cases, the flow is with a developing temperature field since the liquid metal under consideration has a very low Prandtl number (0.02) and heat transfer occurs only near the exit plane. In the case of low-Prandtl number fluids, the thermal boundary layer grows faster than the velocity boundary layer. The thermal diffusivity dominates over the molecular diffusivity. Thermal boundary layer, which is seen to manifest along the window, gets thinner with increasing Reynolds number. The energy is transported through the steeper temperature gradient.

Figure 8 depicts the streamline plots for Re = 500, 700 and 1000 for the target system with nozzle shaped flow guide. Like in the straight flow guide case, the recirculation regions are observed in the inlet section due to expansion of the flow domain and near the exit plane. One may notice the absence of the vortices in the return path along the flow guide with the nozzle-shaped guide. However, prominent vortices are observed at the bottom corner of the downcomer section. The size of the vortices decrease with increase in the Reynolds number. Pressure contours (figure 9) and temperature contours (figure 10) in the case of the target system with nozzle-shaped flow guide show trend similar to those observed in ADSS with a straight flow guide.
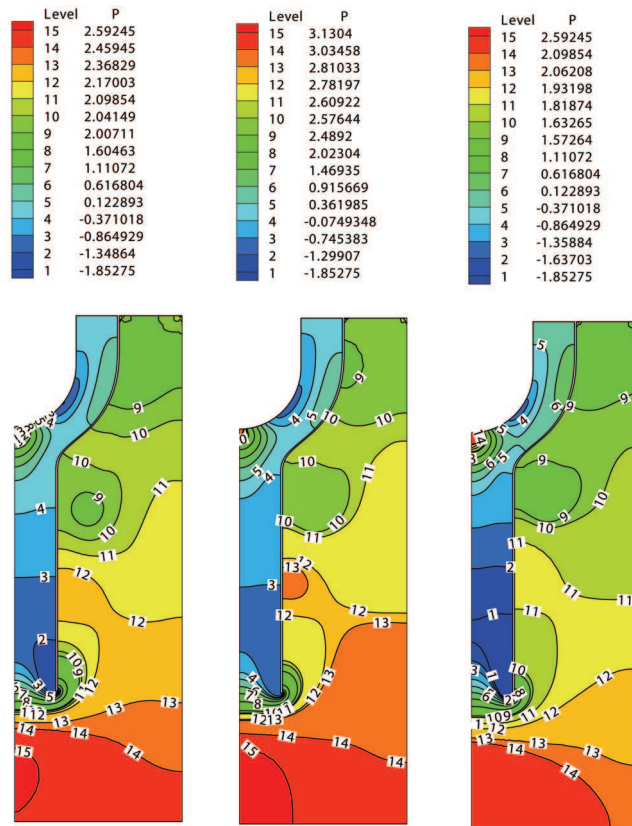
Figure 6. Pressure contours of the target system of an ADSS with straight flow guide for Re = 500, 700 and 1000.

6. Conclusions

A computational study using SUPG-based finite element method has been accomplished to determine the laminar flow and heat transfer characteristics in the target system of complex ADSS geometries with two different types of flow guide. The velocity profile, pressure variation and temperature distribution along the window have been predicted numerically. In both the cases vortices are generated at the smooth backward step near the inlet and at the exit along both the beam window and the guide. The vortices are observed in the return path for the straight guide whereas the recirculation regions are observed at the bottom corner of the down comer section in the nozzle-shaped flow guide case. The vortices noticed in the latter case at the bottom of the downcomer section may be avoided by smoothening the sharp edged bottom wall of it. The size of the primary vortices decrease due to decreasing pressure field for both the cases with the increase in Reynolds number. The dimensionless pressure for all the cases computed show a uniform rise in the backward facing step, drops drastically along the 180° bend, recovers partially up to the leading edge of the window and finally fall to the atmospheric pressure near
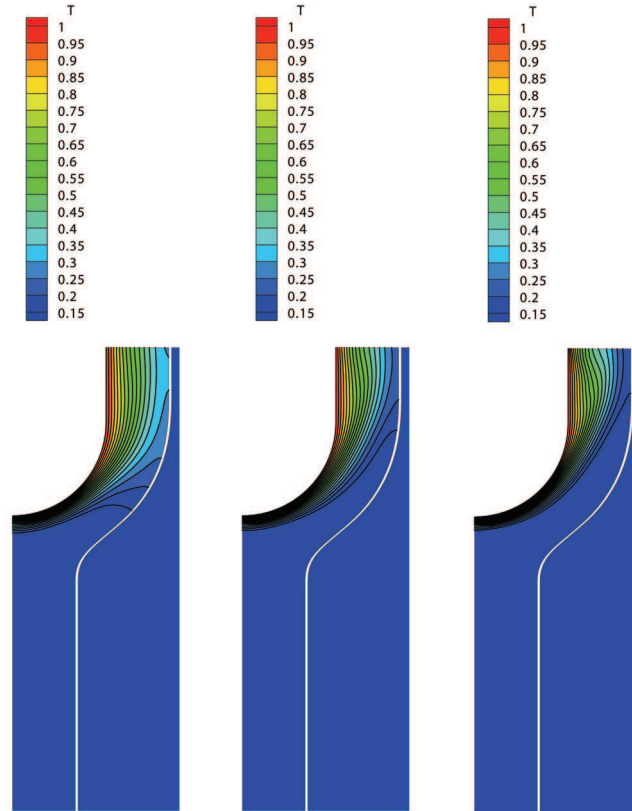
Figure 7. Temperature contours of the target system of an ADSS with straight flow guide for Re = 500, 700 and 1000.

the exit plane. Temperature contours indicate that the amount of heat diffused towards the radial direction decreases and become sharper as more heat is convected towards exit with the increase in the Reynolds number.

Acknowledgments

Nomenclature

C_f Skin friction coefficient
p dimensionless pressure $(=(p)/(\rho)(V_0)^2)$
u, v dimensionless velocity components in x and y directions
         $(=(u)/(V_0),\ (v)/(V_0))$
x, y dimmensionless cylindrical coordinates along the radial and
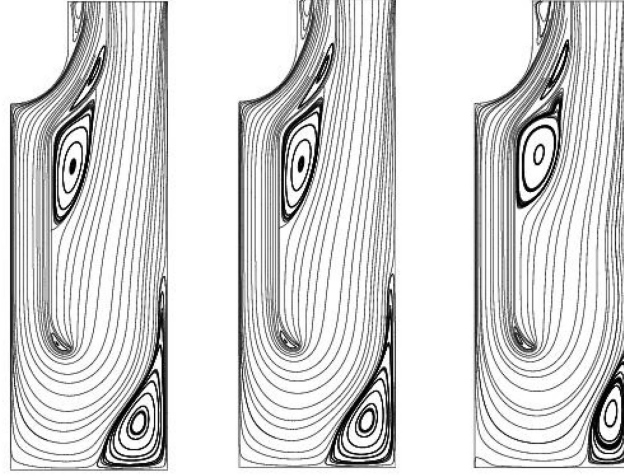   axial directions $(=(x)/(D),\ (y)/(D))$

Figure 8. Streamline plots of the target system of an ADSS with nozzle-shaped flow guide for Re = 500, 700 and 1000.
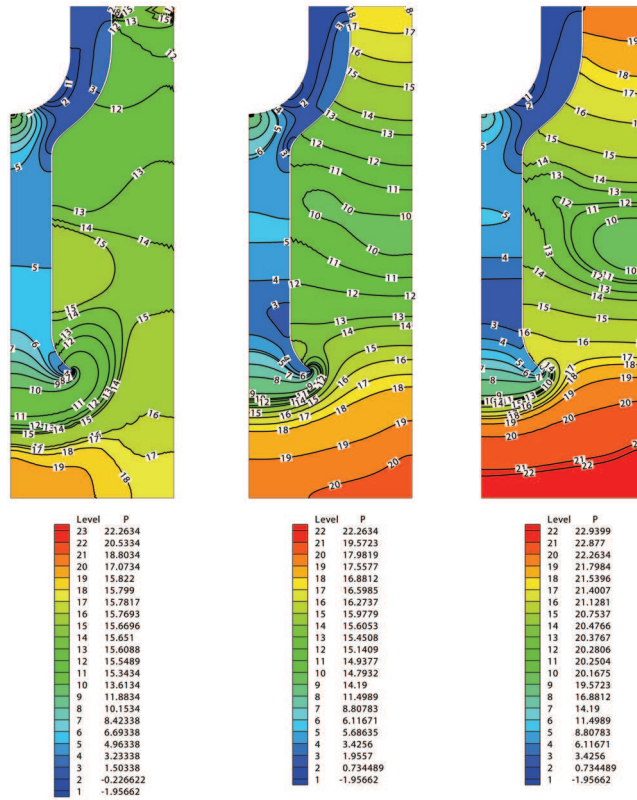

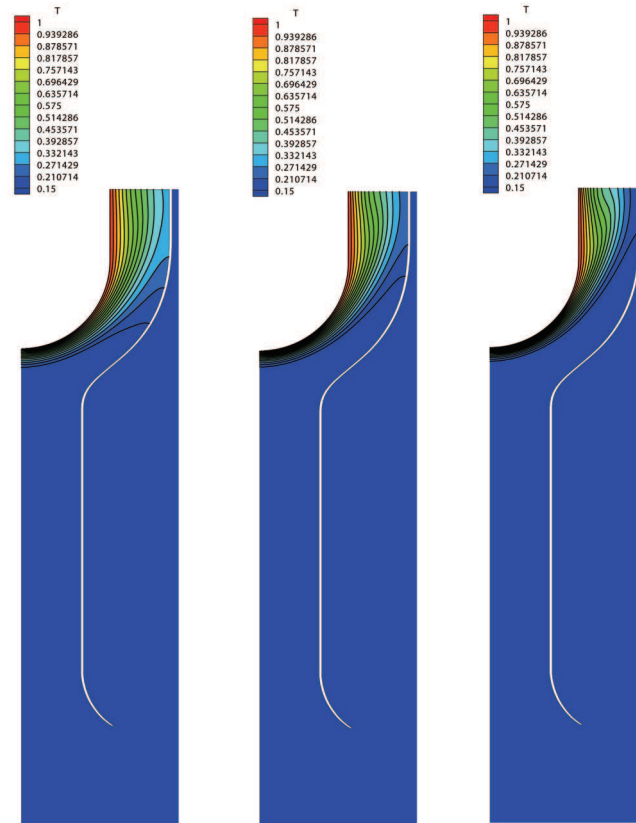**Figure 9.** Pressure contours of the target system of an ADSS with nozzle-shaped flow guide for Re = 500, 700 and 1000.

Figure 10. Temperature contours of the target system of an ADSS with nozzle-shaped flow guide for Re = 500, 700 and 1000.

Greek symbol

θ dimensionless temperature $(= (T - T_\infty)/(T_w - T_\infty))$
ρ density of fluid (kg/m^3)
μ absolute viscosity of fluid $(\text{kg/m} \times \text{s})$
τ dimensionless time $(t/D/V_0))$; t=dimensional time

References

[1] C Rubbia, J A Rubio, S Buono, F Carminati, N Fietier, J Galvez, C Geles, Y Kadi, R Klapisch, P Mandrillon, J P Revol and Ch Roche, Conceptual design of a fast neutron operated high power energy amplifier, CERN Report, CERN-AT-95-44 (ET), Geneva, 29 September 1995

[2] J R Maiorino, A D Santos and S A Pereira, *Brazilian J. Phys.* **33(2)**, 267 (2002)

[3] T V Dury, B L Smith and G S Bauer, *J. Nucl. Technol.* **127**, 218 (1999)

[4] C H Cho, T Y Song and N I Tak, *Nucl. Engg. Design* **229**, 317 (2004)

[5] Batta, C H M Broeders, X Cheng, A Konobeyev, J Neitzel, N Tak and A Travleev, Window target unit for the XADS lead–bismuth cooled primary system, *Proc. of the International Workshop on P and T and ADS Development 2003*, Mol, Belgium, October 6–8

[6] J Chorin, *J. Comput. Phys.* **2**, 12 (1967)

[7] J N Reddy and D K Gartling, *The finite element method in heat transfer and fluid dynamics* (CRC Press, Florida, 1994)

[8] R L Lewis, P Nithiarasu and K N Seetharamu, Fundamentals of the finite element method for heat and fluid flow (John Wiley and Sons, England, 2004)

[9] F H Harlow and J E Welch, *Phys. Fluids* **8**, 2182 (1965)

[10] J Donea, S Giuliani and H Laval, *Comput. Method. Appl. Mech. Engg.* **30**, 53 (1982)

[11] P K Maji and G Biswas, *Int. J. Numer. Meth. Engg.* **45**, 147 (1999)

[12] N Brooks and T J R Hughes, *Comput. Methods Appl. Mech. Engg.* **32**, 199 (1980)